Influence of artificial aging on mechanical properties of commercially and non-commercially available zirconia dental implants

Mona Monzavi, Fei Zhang, Sylvain Meille, Thierry Douillard, Jérôme Adrien, Sammy Noumbissi, Hessam Nowzari, Jérome Chevalier

Influence of artificial aging on mechanical properties of commercially and non-commercially available zirconia dental implants

Mona Monzavi[a,b,*], Fei Zhang[b], Sylvain Meille[b], Thierry Douillard[b], Jérôme Adrien[b], Sammy Noumbissi[c], Hessam Nowzari[a], Jérôme Chevalier[b]

[a] *Private Practice, 120 S Spalding Drive, Beverly Hills, CA, 90212, USA*
[b] *Université de Lyon, INSA-Lyon, UMR CNRS 5510 MATEIS, 7 Avenue Jean Capelle, 69621, Villeurbanne Cedex, France*
[c] *International Academy of Ceramic Implantology Zirconia Implant Research Group-ZIRG, 801 Wayne Avenue, Suite G200, Silver Spring, MD, 20910, USA*

Objective: To evaluate the effect of artificial aging on the mechanical resistance and micromechanical properties of commercially and noncommercially available zirconia dental implants.
Methods: Scanning electron microscopy (SEM) and X-ray computed tomography (X-CT) were performed on implant systems including: Z-systems®, Straumann®, Zibone® and commercially and non-commercially available TAV dental® with varying grain sizes. Accelerated aging was performed at 134 °C and 2-bar pressure for 30 hours. Before and after aging, the mechanical load to failure was investigated and the bending moments were calculated. Nanoindentation responses of the representative Zibone implant before and after aging were per-formed to evaluate the effects of aging on hardness (*H)* and Young's modulus (*E)*. A two-sample *t*-test statistical analysis was used to determine significant differences of bending moments within groups.
Results: All implants presented with compact and homogenous core structures without porosities. The bending moment was significantly increased after aging for all groups ($P \leq 0.05$) except for Z-systems (significant de-crease ($P = 0.022$)) and TAV group 3 (no significant increase ($P = 0.181$)). The increase in bending moment was less pronounced with increasing grain size in TAV groups (group 1: $P = 0.036$, group 2: $P = 0.05$, group 3: $P = 0.18$). *E* and *H* were reduced approximately 32% and 18% respectively following aging within the trans-formed, microcracked zone of the presentative Zibone implant.
Conclusions: Aging led to both increase and decrease of the mechanical properties of the implant systems ana-lyzed. The apparent contrast amongst groups can be explained based on differences in grain sizes and surface features. Aging decreased micromechanical properties of one implant system which warrants further in-vestigation.

1. Introduction

Dental implant therapy is a widely accepted treatment modality in the rehabilitation of partially and fully edentulous patients (Branemark et al., 1977; Alberktsson et al., 2007). Titanium is the most prevalent implant material and has been considered the gold standard with a 10–15 year survival rate of above 90% (Alberktsson et al., 2007; Van Velzen et al., 2015; Branemark et al., 1969; Adell et al., 1981). Despite the proven clinical success of titanium, its aesthetic outcome can be compromised in cases of thin peri-implant mucosa or soft tissue recession. Furthermore, titanium and titanium alloy implants are vulnerable to corrosion in the oral environment, and as a consequence, they release metal ions into peri-implant soft and hard tissues (Luciana et al., 2017). Ceramic implants have gained increased popularity due to their improved aesthetic properties (Andreiotelli et al., 2009).

Within the past decade, the biomechanical properties of ceramic implants have been enhanced based mostly on the introduction of partially yttria-stabilized zirconia (Y-PSZ) (Piconi and Maccauro, 1999), owing to a phase transformation toughening mechanism (Christel et al., 1989). Y-PSZ are most often referred to as 'tetragonal zirconia polycrystal' (Y-TZP) in the dental field. Available load stimulation data on one-piece Y-TZP oral implants has shown a range within the limits of clinical requirements (Kohal et al., 2011). Regardless, in presence of moisture and lack of mechanical stress, the metastability of Y-TZP may lead to a spontaneous transformation of grains from a tetragonal to a monoclinic (t-m) phase at the surface, which continues to

* Corresponding author. Private Practice, 120 South Spalding Drive, Suite 201, Beverly Hills, CA, 90212, USA.
E-mail address: monzavi.mona@gmail.com (M. Monzavi).

the bulk of the material (Kobayashi et al., 1981; Chevalier et al., 2009a). This physical mechanism occurs at much lower temperatures (65 °C–300 °C) than it normally occurs (1000 °C) and is referred to as low temperature degradation (LTD) or aging (Kobayashi et al., 1981). Transformation first occurs at a specific grain on the surface that is more susceptible to the phase transformation because of a disequilibrium state, which may include lower content of stabilizer, presence of residual stress or a large grain size (Chevalier, 2006). Since the transformation is accompanied by volume expansion of crystalline structure, it causes surface uplift and micro cracks, which leads to surface roughening and grain delamination (Kobayashi et al., 1981; Chevalier et al., 2009a). Despite numerous attempts, the exact mechanism of slow t-m transformation triggered by water molecules is still under question (Chevalier et al., 2007). Nevertheless, the following steps have been proposed (Chevalier et al., 2009a; Yoshimura et al., 1987; Lawson, 1995):

- Chemical adsorption of H_2O on ZrO_2 surfaces
- Formation of Zr–OH bond disrupting Zr–O–Zr bond
- Penetration of OH^- and/or O^{2-} into the inner part by grain boundary diffusion
- Filling of oxygen vacancies by OH^- and/O^{2-}
- Reduction of the oxygen vacancies destabilizing tetragonal phase

Y_2O_3 is the most widely used stabilizer, and typically 3 mol % is used to stabilize the tetragonal phase at room temperature (Lughi and Sergo, 2010). Increasing the Y_2O_3 content improves the resistance to LTD, but it can also inhibit the t-m transformation, thus decreasing the mechanical properties of the material (Tsubakino et al., 1991). Doping Y-TZP with other oxides, specifically alumina (~0.25 wt%), has been shown to provide a satisfactory balance between aging resistance and mechanical properties (Chevalier et al., 2009b; Keuper et al., 2013).

Chemical stabilization, stress and grain size are interlinked and affect one another in a complex way. It has been established that an increase in the content of chemical stabilizer induces a reduction in the grain size, which has a beneficial effect on the stability of the tetragonal phase and resistance to LTD (Lughi and Sergo, 2010). However, decreasing the grain size may also reduce the stress-induced transformation and lead to a decrease in fracture toughness mainly because of less efficient phase transformation toughening, while a larger grain size leads to higher local stress (Lughi and Sergo, 2010; Cattani-Lorente et al., 2011). In addition to the above factors, different surface textures to improve osseointegration may influence mechanical strength, fatigue and aging resistance (Karakoca and Yilmaz, 2009; Curtis et al., 2006).

A recent evaluation has shown that aging effects each implant system differently based on variations on the surface microstructural properties and grain size (Monzavi et al., 2016). Today, only a few available studies exist on the influence of aging on the mechanical properties of zirconia implants. The majority of data are extracted from 20-year-old literature in the orthopedic field (Chevalier et al., 2007). As a general trend, it is known that microcracking may lead to a decrease of surface micromechanical properties (Cattani-Lorente et al., 2011). With regard to its effect on strength, the results are variable, as both an increase (Sanon et al., 2013; Chevalier et al., 2011; Marro and Anglada, 2012) and a decrease (Borchers et al., 2010) in strength have been reported for zirconia implants with different surface treatments.

Regardless, as previously suggested, each implant system with its unique microstructural properties, geometry and surface treatment should be evaluated via an accelerated aging test prior to its use in a clinical setting (Sanon et al., 2015). This is important when considering the effect of LTD on specific batches of Y-TZP femoral heads which led to microcracking and surface delamination of the grains (Clarke et al., 2003).

In part I of this investigation submitted for publication, we evaluated the influence of accelerated aging on commercially and non-commercially available zirconia dental implants with varying surface treatments, grain sizes and microstructural properties before and after aging. The current investigation aims to evaluate the influence of LTD on fracture resistance, elastic modulus and hardness of the same groups of commercially and noncommercially available Y-TZP (Yttria stabilized tetragonal zirconia polycrystal) implants with varying microstructural properties before and after accelerated aging. The kinetics of LTD is thought to be highly dependent on the processing conditions and the resulting microstructure of the material. For instance, it is widely accepted that large grain size as a result of high sintering temperatures generally triggers transformation. Similarly, low density and open porosities due to incomplete sintering allow water to diffuse towards greater depth and increase susceptibility to LTD (Chevalier et al., 2007, 2009a). Thus, Grain size and sintering conditions are known to be the primary factors influencing the LTD kinetics of zirconia ceramics (Chevalier et al., 2009a; Lughi and Sergo, 2010; Inokoshi et al., 2014). However, to the best of the authors' knowledge, this has not been studied for dental implants. Thus, the present study also aims to evaluate the influence of increase in grain size due to subtle changes in the sintering process on fracture resistance of zirconia implants with some non-commercially available specimen.

The null hypotheses of the present study are as follows:

- LTD does not influence the mechanical and micromechanical properties of Zirconia dental implants.
- Increase in grain size is not correlated to increase in bending moment following aging.

2. Materials & methods

2.1. Implant description

One-piece Y-TZP ceramic commercially available and prototype zirconia dental implants were provided by the manufacturers. Table 1 summarizes the implants and their manufacturing processing. Although all implants shared the common feature of being made from 3 mol % yttria-stabilized zirconia powder, each implant system was processed differently.

Z-systems® (Oensingen, Switzerland) surface treatment consisted of sand blasting and laser modification with a patented laser process SLM® (surface laser modified). Implants had a screw design shape with a tapering thread and widened core diameter in the upper part of the thread. The implant dimensions consisted of a shoulder diameter of 6.0 mm, an outer diameter of 5 mm and lengths of 8 and 12 mm. Straumann® (Basel, Switzerland) monotype full ceramic implant processing consisted of powder preparation, spray drying, cylinder pressing, sintering, HIP (heat isostatic pressing), machining, sand blasting and etching with hydrofluoric acid. Implants had a tissue level platform with a 1.8 mm transmucosal neck, a 4.8 mm shoulder diameter, a cylindrical screw design endosseous part and a coronal tapered thread core diameter. The outer diameter, including the threads, was 4.1 mm, the thread pitch was 0.8 mm, the abutment height was 5.5 mm, and the total endosseous length was 12 mm. Zibone® (Luzhu Dist Taoyuan, Taiwan) full ceramic implants were processed via injection molding, sintering, grinding, and sandblasting. Surface treatment consisted of sand blasting the surface using zirconia sand. Implants had an outer diameter of 4 mm and a total endosseous length of 10 mm. TAV Dental® (Shlomi, Israel) implants consisted of 3 groups with different grain sizes. Group 1, with a grain size of 0.4 μm, is commercially available. Group 2 (grain size: 0.49 μm) and group 3 (grain size: 0.6 μm) were prototypes, for which the sintering temperature was intentionally increased to investigate the effect of grain size on aging kinetics. All three groups of implants had diameters of 4.1 mm and lengths of 8 mm. Similar to ZiBone, TAV implants were manufactured by means of ceramic injection molding, and their surfaces are sintered following injection molding.

Table 1

	Initial powder, Process history	Grain size of zirconia	Sand blasting	Etching	Laser treatment	Additional treatment	Sterilization
Z-Systems®, Z5c Zirkolith®, Oensingen, Switzerland	TZP-A Isostatic compaction, sintering, HIP, grinding	0.4 µm	Al_2O_3[a]	No	SLM patented	Sintering	Plasma sterilization
Straumann® Pure Ceramic Implant, Basel, Switzerland	TZP-A, spray drying, Cylinder pressing, sintering, HIP, machining	0.22 µm[a]	ZrO_2 Large grit	Hydrofluoric acid	No[a]	No information	No Information
Zibone®, Coho Biomedical Technology Co. Ltd, Taiwan	TZP-A, Injection molding, sintering, grinding	0.39 µm[a]	ZrO_2	No	No[a]	Annealing[a]	No information
TAV Dental®, Shlomi, Israel	TZP-A, Injection molding, sintering	0.4/0.49/0.6 µm	No information	No information	No[a]	No information	No information

[a] Information was obtained in this study. The remaining information obtained from manufacturer.

2.2. SEM analysis

Surface microstructural topography was examined using SEM to characterize surface features specific to each implant system. These experiments were performed using a FIB/SEM workstation (NVision 40; Carl Zeiss Microscopy GmbH, Oberkochen, Germany).

2.3. X-ray tomography

X-ray tomography (phoenix® X-ray, GE Sensing & Inspection Technology, Wunstorf, Germany) was conducted on one sample from each manufacturer to assess the presence of porosity within the core of each implant system. The equipment is built inside a lead self-protected cabin, which allows *in situ* devices to be installed inside. The X-ray source is an open transmission nanofocus X-ray tube that can be operated at accelerating voltages ranging from 40 to 160 kV. The thin transmission target hit by focused electrons is made of tungsten or molybdenum depending on the energy range required to image the sample. This tube delivers a cone X-ray beam with a focus size that can be tuned between 1 and 6 µm. The detector is a Paxscan™ amorphous silicon flat panel. It is composed of 1.920 rows and 1.536 lines of square sensitive pixels (127 x 127 μm^2) and can be used in a 1 × 1 or 2 × 2 binning mode. The detector delivers the value of the attenuation with a 14-bit gray-level coding resolution. The maximum voxel size is approximately 170 µm in binning mode and when the sample stage is placed close to the detector. The minimum voxel size (on the order of 0.6 µm) is obtained when the sample is the closest possible to the source. In practice, the minimum resolution ever obtained in a tomographic scan using this set up is approximately 1.5 µm with a voxel size of 0.7 µm. The parameters for our investigation included a scan time of 20–35 min at an accelerating voltage of 155 kV, a current of 60 µA, a 4–10 µm voxel size, an exposure time of 667 m s and 500–800 projections.

2.4. Accelerated aging test

Implants were artificially aged for 30 hours (n = 30, n = 5 each group) at 134 °C under 2-bar pressure in a conventional dental autoclave. Prior to increasing the temperature, atmospheric air was evacuated to ensure 100% humidity. Ageing in autoclave has often been used as a tool to accelerate ageing and to assess the resistance to LTD of a given 3Y-TZP based material. It is used in ISO recommendations, which requires no more than 25 vol% of monoclinic phase measured by X-Ray diffraction after 5 hours at 134 °C, 2 bars. From time-temperature equivalence and the knowledge of the activation energy of LTD at relatively low temperature, it has been calculated and often considered that 1 h in autoclave at 134 °C would be roughly equivalent to 1–4 years at 37 °C (Sanon et al., 2015). The conditions explored in this study would consequently represent long term duration at 37 °C.

2.5. Nanoindentation

Nanoindentation was performed on mechanically polished cross sections of Zibone® implants in aged and non-aged regions to evaluate the elastic modulus and hardness using a nanoindenter (Agilent G200, Agilent Technologies, USA). Sample preparation included nickel plating to protect the samples' surface from machining damage. After nickel electroplating, the implant was sectioned in the middle with a water-cooled diamond wire saw (Model 3242, Well, Switzerland) and embedded in epoxy resin. The cross sections of the samples were then sequentially ground with 40, 20, and 10 µm diamond discs and polished with 7, 3, and 1 µm diamond pastes. A final chemical-mechanical polishing lasting a few minutes was performed with colloidal silica on an EcoMet250 (Buehler, LakeBluff, IL, US). Instrumented indentation tests with a maximum penetration depth of 400 nm were carried out at a constant strain rate of 0.05 s^{-1}. A fused silica sample was used to

calibrate the Berkovich diamond tip. The continuous stiffness measurement (CSM) method was utilized to calculate the hardness (H) and Young's modulus (E) evolution with penetration depth during the loading phase. Ten indentations were placed on the polished cross section in the transformed zone (aging of 30 h) and the nontransformed zone characterized from our surface SEM investigation (Fig. 4). The location of indentations was checked with optical microscopy following indentation testing.

2.6. Mechanical characterization

Each type of implant was characterized in terms of load to failure before (n = 5) and after (n = 5) accelerated aging duration for 30 hours at 134 °C in water steam and 2 bar pressure. The objective was to determine the possible impact of surface modification due to aging on a given type of implant but not to compare different types of implants in terms of their mechanical strength, as each implant system is different in terms of design, geometry, processing and surface modification. Load to failure tests were performed according to the ASTM standard (ISO 14801). Implants were embedded in an epoxy resin (RenCast CW 20/HY 49) held by individually custom-made Teflon molds for each implant type at axial angulation (90°) with respect to the horizontal axis. To simulate bone resorption, the implants were embedded in resin just to the 3rd thread from the top. Once the resin had set, the samples were removed from the Teflon mold and placed in the implant holder at a 30° angle with respect to the vertical axis. After mounting the implant holder onto the INSTRON 8502 testing machine, the configuration was set to apply a load to a strain rate of 2 mm/min to limit slow crack growth during loading. Our evaluation follows geometry from a method adapted from ISO 14801 (Sanon et al., 2015).

2.7. Statistical methods

The load to failure average and standard deviation values of all groups in the as-received state and after 30 hours of artificial aging were measured. The bending moment was calculated at the time of implant fracture, which included the lever arm extension [cm] multiplied by the fracture load [N].

The two-sample *t*-test was used to compute significant differences within each group before and after aging at a p value of 0.05 using statistical analysis software (Minitab® 16.2.1, Pennsylvania, USA). Significant differences within each group before and after aging were set at the level of alpha = 0.05.

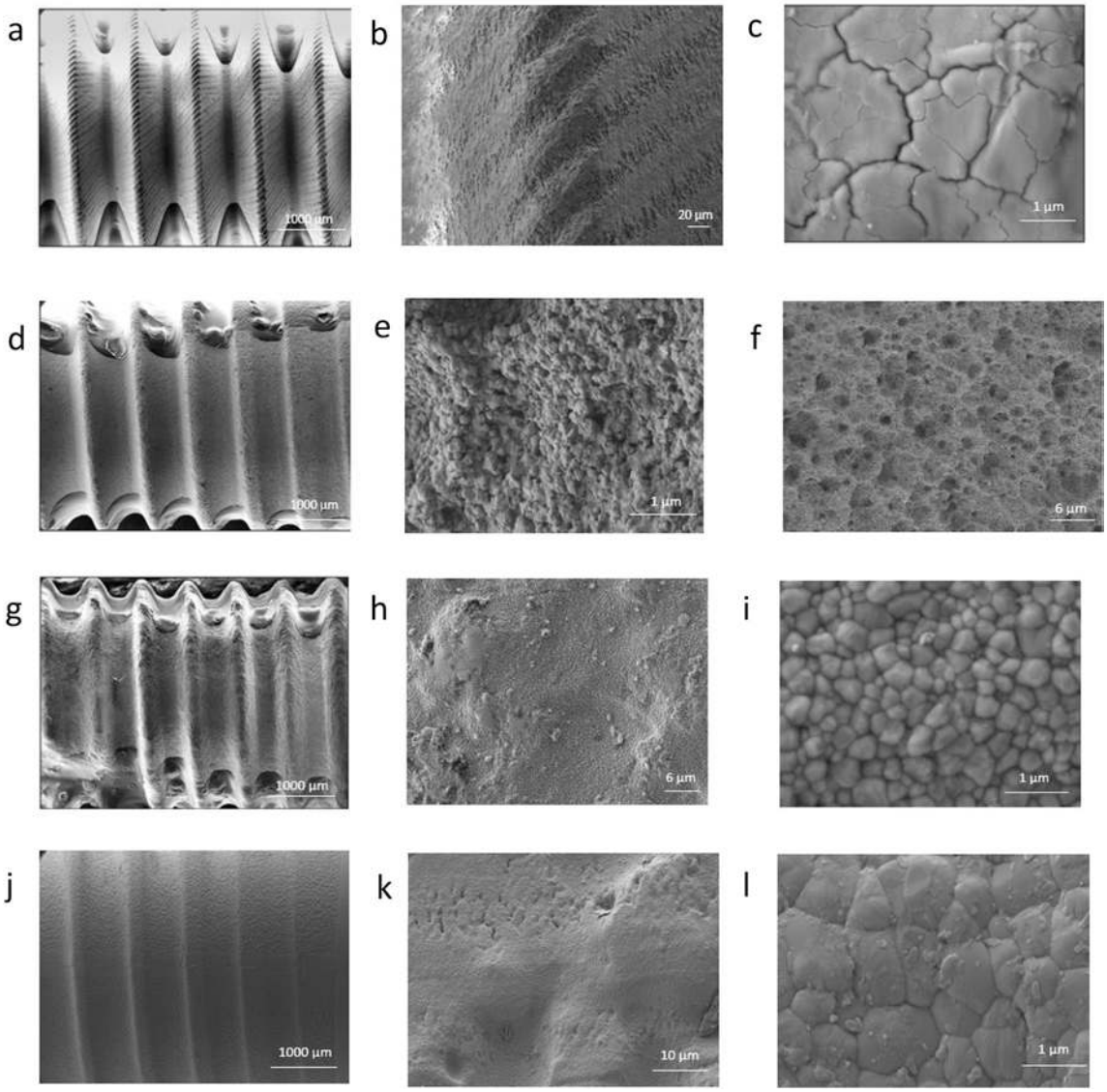

Fig. 1. Surface SEM images of thread portions of implants at different magnifications. (a–c) Z-systems®, (d–f) Straumann®, (g–i) ZiBone®, (j–l) TAV Dental®.

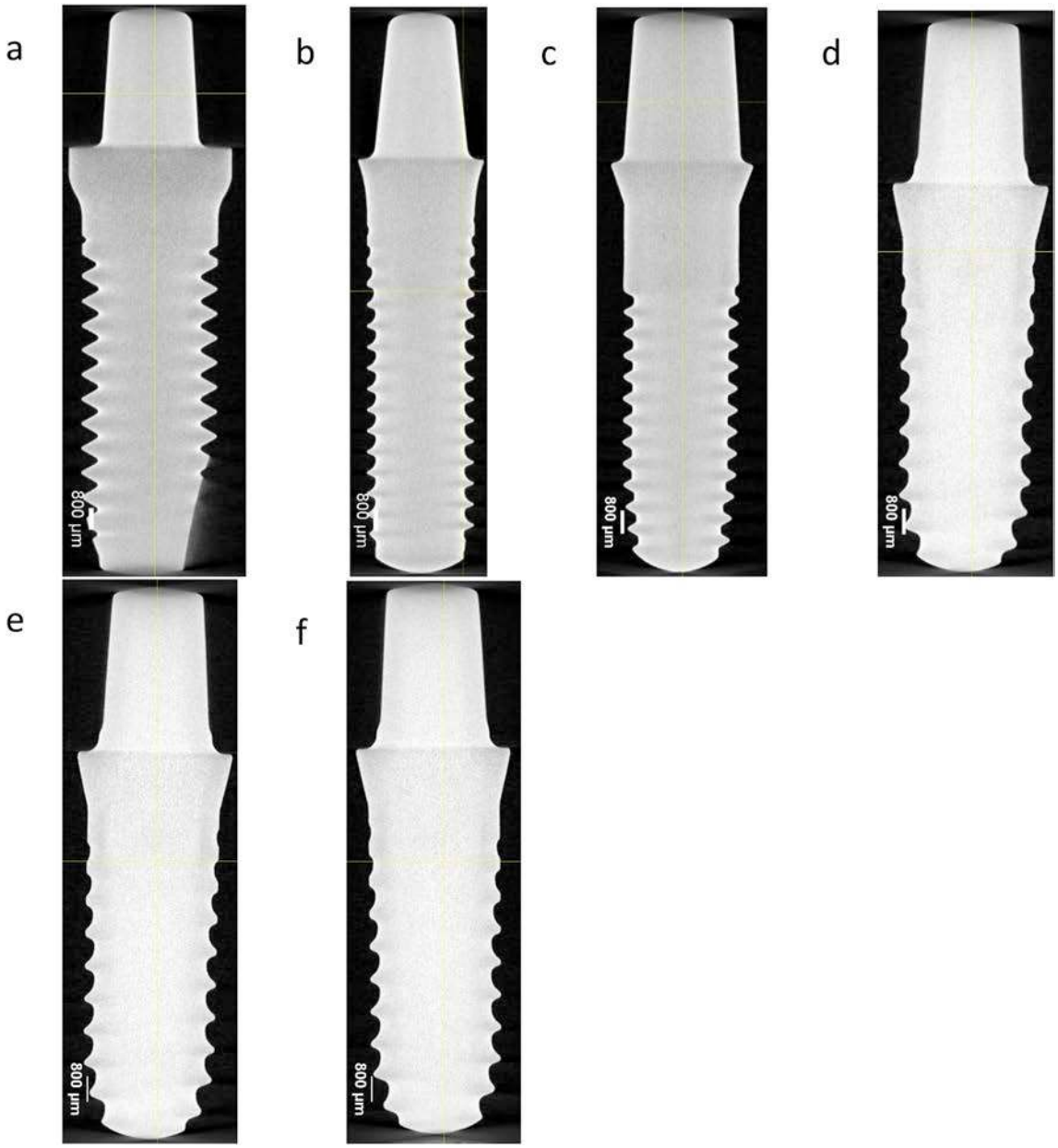

Fig. 2. Slice of X-ray tomography volumes. (a) Z-systems, (b) Straumann, (c) ZiBone, (d) TAV group 1, (e) TAV group 2, (f) TAV group 3.

3. Results

3.1. Surface and core microstructural features of implants

Surface SEM images are presented in Fig. 1. The Z-systems® implant had a v-shaped thread design with rounded edges and a melted surface structure from laser treatment characterized by symmetrical parallel grooves at the crest of the threads. High magnification of the grooves showed numerous microcracks as a result of laser treatment. The Straumann® implant had a buttress-shaped thread design with sharp square edges and nonsymmetrical sides. The surface presented with macroporous valleys and microrough pits. At higher magnification, the surface presented with a homogeneous grainy structure. The Zibone® implant presented with a v-shaped thread design, rounded edges and symmetrical sides. Surface features presented with an increase in grain size in most areas due to annealing and flattened surfaces in other areas as a result of sandblasting via zirconia sand. The TAV Dental® implant presented with square-threads. The surface appeared to be sintered directly following the injection molding with no further surface treatment. At low magnification, numerous pores were visible. At high magnification, a grainy structure with parallel lines was evident, indicating grain transformation (Fig. 1). X-ray tomography 3D scans did not show major porosity within the core of each implant system (see Fig. 2 for cross sectional slice). With the detection limit of the configuration used in this work, the observations demonstrated that no defect larger than a dozen microns was present in the implants provided.

3.2. Elastic modulus and surface hardness

Nanoindentation load-displacement curves as well as hardness H and Young's modulus E versus penetration depth curves of a polished section of Zibone® implant obtained in nontransformed and transformed zones after accelerated aging are displayed in Fig. 3. This specific implant system was chosen for this evaluation as it presented with a well-defined transformation zone revealed by microstructural evaluation and a noticeable change in mechanical properties following aging. The average moduli of elasticity and hardness are listed in Table 2. The initial values of the elastic modulus and hardness below

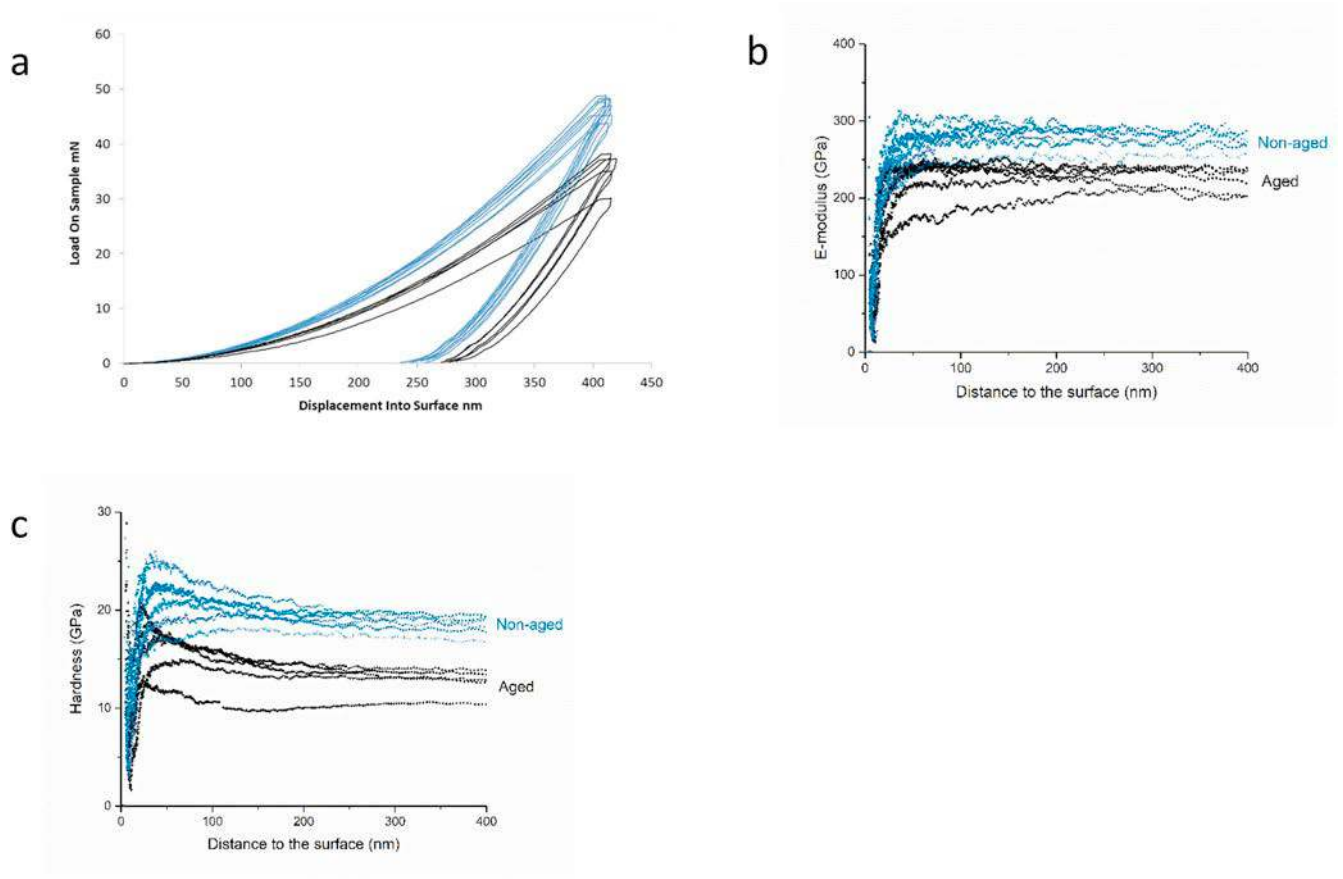

Fig. 3. Load-displacement curves for aged (black) and nonaged (blue) regions (a), elastic modulus (b) and hardness (c) as a function of penetration depth in nonaged and aged zones of ZiBone implants at 30 h.

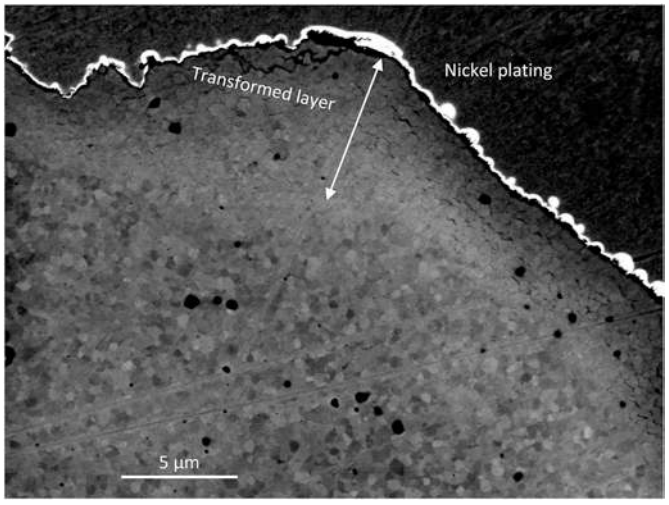

Fig. 4. SEM image of ZiBone polished cross section presenting the transformed zone where the indentations were made.

100 nm of penetration depth are affected by the surface roughness of the sample and should not be taken into account. Accelerated aging led to a decrease in both *E* and *H*. Overall, reduced hardness and Young's modulus of approximately 32% and 18%, respectively, were observed in the transformed zone.

3.3. Mechanical properties of as-received and aged implants

Load to failure and bending moment values are presented in Table 3. The bending moment values significantly increased following aging in Straumann®, TAV® group 1, TAV® group 2 and Zibone® ($p < 0.05$). TAV® group 3 presented with an increased bending moment following aging, which was not statistically significant. For the Z-systems®, the bending moment was significantly reduced following aging. The bending moment increased with increasing grain size in the TAV® groups.

Table 2
Elastic modulus (E) and hardness (H) in nontransformed and transformed zones, ZiBone implant.

	E (GPa)	H (GPa)
Non-aged	278 ± 19	19 ± 1
Aged (30 h)	228 ± 13	13 ± 1

4. Discussion

In the present study, the effect of aging on the mechanical and micromechanical properties of commercial and noncommercialized zirconia dental implants was examined. Artificial aging was performed on the actual surface of implants rather than bending bars/discs. Our evaluation used a procedure based on the ISO 14801, which dictates the simulation of a 3 mm bone recession. In addition to fracture load, bending moment values were calculated because it is more relevant to use bending moments when comparing different investigations with diverse methodologies. The mean bending moment values for all implant systems following aging ranged from 307 to 464 NCm, which is slightly larger than previous reports (Spies et al., 2016). The bending moment was increased in all groups after aging except for the Z-systems

Table 3
Average measurements (bending moment, fracture load) at an embedding angle of 30° for different test groups including comparison (two-sample *t*-test) of as-received and aged samples with respect to their bending moment within in the groups.

Group	N	Bending moment (Nmm) Sign. (t-test)	mean	SD	Fracture load (N) mean	SD
Z-systems (0 hr)	5	0.02*	4530	336	846	76
Z-systems (30 hr)	5		3970	260	747	63
Straumann (0 hr)	5	0.04*	4112	407	748	57.6
Straumann (30 hr)	5		4644	253	910	70
ZiBone (0 hr)	5	0.004*	2400	288	366	49
ZiBone (30 hr)	5		3072	200	482	25
TAV 0.4 µm (0 hr)	5	0.036*	3544	196	628	23.5
TAV 0.4 µm (30 hr)	5		4010	221	718	44.4
TAV 0.49 µm (0 hr)	5	0.05*	3653	252	651	50
TAV 0.49 µm (30 hr)	5		4086	322	737	66.8
TAV 0.6 µm (0 hr)	5	0.18	3922	205	698	53
TAV 0.6 µm (30 hr)	5		4189	319	747	57

*Statistically significant difference compared to the as-received group

*Statistically significant difference compared to the as-received group.

in which the bending moment was significantly reduced following aging. A previous report (Spies et al., 2016) has shown a decrease in the bending moment of Y-TZP machined surface two-piece implants following aging. A decreased flexural strength of Y-TZP standardized disc specimens following aging was also reported in another investigation (Kohorst et al., 2012), while another report showed an increase in load to failure values following aging of injection molded Y-TZP implants (Sanon et al., 2015). In this specific study (Sanon et al., 2015), one group had a structured rough surface (implants called 'Axis-rough'), while another had an additive surface with an additional proprietary porous zirconia coating (implants called 'Axis-alveolar'). The Axis-rough group had a continuous increase in load to failure following aging at 5 and 100 hours for up to 730 N at 100 hours. The Axis-alveolar implant had an increase in load to failure at 5 hours (431 N), while the value decreased at 100 hours to 417 N (Sanon et al., 2015). Evaluating our results and those of previous investigations, it is difficult to deduce whether a specific factor may be more crucial in influencing mechanical properties following aging. The variability of results among different investigations provides further evidence that each implant system with its unique surface treatment, shape, processing and material content can behave differently in its mechanical properties following aging. When combining the present set of data with our previous microscopy analysis, it may be deduced that implant systems with less surface treatment such as TAV, Zibone and Straumann had reduced transformation to start with, which led to less compressive stress among grains at the surface. Following aging, compressive stress increased as a result of t-m transformation, which may be a factor leading to increased bending moments. In Z-systems, the laser-treated surface created a zone of transformation with compressive stress, which led to a higher bending moment in the as-received group compared to the aged group. Following aging, the quantity of microcracks may have disturbed the balance between compressive stress and microcracks, which led to an overall reduction in bending moment values. Furthermore, TAV group evaluation provided evidence that increased grain size leads to higher transformation and increased compressive stress following aging, which results in higher bending moment values. X-ray tomography results largely revealed a dense microstructure in the absence of large porosities for all samples. Zibone implants presented with microporosity within the core of polished cross sections. This porosity may account for significantly reduced bending moments in this group before and after aging.

Nanoindentation was used to evaluate the change in the surface micromechanical properties at a local scale following aging by calculating the hardness and Young's modulus with penetration depth. The polished cross section of the Zibone group presented with the most uniform separation zone between transformed and nontransformed areas, allowing for more precise evaluation of the properties of the two zones. Values of surface E and H were within the same range but slightly higher than previous reports in both transformed and non-transformed zones (Cattani-Lorente et al., 2014; Gailard et al., 2008). It has been shown that artificial aging results in a decreased elastic modulus and hardness (Guicciardi et al., 2007; Cattani-Lorente et al., 2011), which has been related to increased aging time (Gailard et al., 2008) followed by a higher proportion of the monoclinic phase (Cattani-Lorente et al., 2011) and microcracking (Jimenez-Pique et al., 2012). Our data confirmed these results, as reduced elastic modulus and hardness were observed in the microcracked zone in the transformed region.

The greater decrease measurement for hardness compared to Young's modulus after aging can be explained by the size of the plastic and elastic zones during indentation testing. Using the model proposed by Chen and Bull (2006), the size of the plastically affected zone can be estimated as 3.6 times the value of the residual penetration depth, using E and H values determined for nonaged Zibone implants. In the tests performed in this work, the residual penetration depth after unloading was 255 and 280 nm for nonaged and aged regions, respectively, leading to an average plastic zone size for both zones of 1 µm. The size of the elastic zone is much larger and represents at least ten times the maximum penetration depth (400 nm) during indentation (Lawn, 1993). The average thickness of the transformed zone on the polished cross section of Zibone® following 30 hours of aging was measured to be between 4 and 6 µm (Fig. 4). The plastic zone is thus clearly contained inside the transformed zone, whereas the elastic affected zone is of the same order of magnitude as the transformed zone. As the microcrack density is not homogenous in the transformed zone but is more important towards the surface of the implant, this could explain that the decrease in properties after aging is stronger for hardness than for Young's modulus.

It is important to note that nanoindentation testing tends to close microcracks due to the presence of compression stresses under the indentation tip. In addition, despite the decrease in the micromechanical properties of the aged zone, the bending moment of this implant system increased following aging due to compressive stresses generated by the transformation. Therefore, the limited decrease in elastic modulus and hardness may not be relevant to clinical applications. This observation needs to be further investigated. The implication of a small microcracked zone at the very near surface might be the subject of future investigation in terms of bone integration before concluding on any adverse effects.

Finally, our findings on the mechanical properties of the currently investigated implants following artificial aging validate the functionality and safety of the evaluated products for clinical applications. Although the ISO 14801 does not define the minimum value for fracture strength, taking the highest clinically measured bending moment of 95 Ncm into account (Morneburg and Pröschel, 2003) and applying a safety buffer of 100%, it is suggested by the authors that a minimum static load to fracture of 200 Ncm for all tested specimen, roughly corresponding to 400 Ncm when embedding the implants according to ISO 14801, might result in clinical safety. However, one is reminded that compared to titanium alloy (fracture toughness of 40–50 MPa $m^{1/2}$), Y-TZP is more brittle with a fracture toughness of 9–12 MPa $m^{1/2}$,

and despite of that, titanium dental implant fractures have been reported (Boutz et al., 1995; Osman and Swain, 2015). In addition, radiological artifacts by zirconia implants provides shortcomings of the material for clinical applications (Kuusisto et al., 2015). Therefore, each case should be precisely evaluated and carefully treatment planned according to patient's conditions and treatment needs.

5. Conclusions

- Artificial aging for a duration of 30 hours resulted in the following:
  - Increased bending moment in TAV, Zibone, and Straumann
  - Decreased bending moment in Z-systems
  - Increased bending moment with increased grain size in the TAV group
- X-ray tomography analysis revealed a dense core structure for all implant types
- Nanoindentation resulted in decreased modulus of elasticity and hardness in the transformed zone as compared to the non-transformed one, which may not be clinically relevant and warrants further investigation
- All implants presented with sufficient fracture resistance to be used for clinical applications.

Conflicts of interest

Authors have no conflict of interest.

Acknowledgements

This study was supported by Institute National des Sciences Appliquées de Lyon research funds. A part of the funds was also provided by the European Commission, under the project H2020 SISCERA (contract number 737954). We would like to thank Z-systems, Straumann, TAV Dental, and ZiBone ceramic implant companies for providing zirconia dental implants, the CLYM (Centre Lyonnais de Microscopie: www.clym.fr) for providing access to their microscopy facilities and Nicolas Vaché for assisting us with nickel electroplating. The authors have no conflict of interest.

Appendix A. Supplementary data

Supplementary data to this article can be found online at https://doi.org/10.1016/j.jmbbm.2019.103423.

References

Adell, R., Lekholm, U., Rockler, B., Branemark, P.I., 1981. A 15-year study of osseointegrated implants in the treatment of the edentulous jaw. Int. J. Oral Surg. 6, 387–416.
Alberktsson, T., Gottlow, J., Meirelles, L., Ostman, P.O., Rocci, A., Sennerby, L., 2007. Survival of NebelDirect Implants: an analysis of 550 consecutively placed implants at different clinical centers. Clin. Implant Dent. Relat. Res. 2, 65–70.
Andreiotelli, M., Wenz, H.J., Kohal, R.J., 2009. Are ceramic implants a viable alternative to titanium implants? A systematic literature review. Clin. Oral Implant. Res. 20, 32–47.
Borchers, L., Stiesch, M., Bach, F.W., Buhl, J.C., Hubsch, C., Kellner, T., Kohorst, P., Jendras, M., 2010. Influence of hydrothermal and mechanical conditions on the strength of zirconia. Acta Biomater. 6, 4547–4552.
Boutz, M.M.R., Winnubst, A.J.A., Van Langerak, B., et al., 1995. The effect of ceria co-doping on chemical stability and fracture toughness of Y-TZP. J. Mater. Sci. 30, 1854.
Branemark, P.I., Adell, R., Breine, U., Hansson, B.O., Lindstrom, J., Ohlsson, A., 1969. Intra-osseous anchorage of dental prostheses. I. Experimental studies. Scand. J. Plast. Reconstr. Surg. 2, 81–100.
Branemark, P.I., Hansson, B.O., Adell, R., et al., 1977. Osseointegrated implants in the treatment of edentulous jaw. Experience from a 10-year period. Scand. J. Plast. Reconstr. Surg. Suppl. 16, 1–32.
Cattani-Lorente, M., Scherrer, S.S., Ammann, P., Jobin, M., Wiskott, H.W., 2011. Low temperature degradation of a Y-TZP dental ceramic. Acta Biomater. 7, 857–865.
Cattani-Lorente, M., Scherrer, S.S., Durual, S., Sanon, C., Douillard, T., Gremillard, L., Chevalier, J., Wiskott, A., 2014. Effect of different surface treatments on the hydrothermal degradation of a 3Y-TZP ceramic for dental implants. Dent. Mater. 1136–1146.
Chen, J., Bull, S.J., 2006. On the relationship between plastic zone radius and maximum depth during nanoindentation. J. Surf. Coat. 201, 4289–4293.
Chevalier, J., 2006. What future for zirconia as a biomaterial? Biomaterials 27, 535–543.
Chevalier, J., Gremillard, L., Deville, S., 2007. Low-temperature degradation of zirconia and implications for biomedical implants. Annu. Rev. J. Mater. Res. 37, 1–32.
Chevalier, Jerome, Gremillard, Laurent, Virkar, Anil V., Clarke, David R., 2009a. The tetragonal-monoclinic transformation in zirconia: lessons learned and future trends. J. Am. Ceram. Soc. 92, 1901–1920.
Chevalier, J., Gremillard, L., Virkar, A.V., Clarke, D.R., 2009b. The tetragonal-monoclinic transformation in zirconia: lessons learned and future trends. J. Am. Ceram. Soc. 92, 1901–1920.
Chevalier, J., Loh, J., Gremillard, L., Meille, S., Adolfson, E., 2011. Low-temperature degradation in zirconia with a porous surface. Acta Biomater. 7, 2986–2993.
Christel, P., Meunier, A., Heller, M., Torre, J.P., Peille, C.N., 1989. Mechanical properties and short-term in-vivo evaluation of yttrium-oxide-partially-stabilized zirconia. J. Biomed. Mater. Res. 1, 45–61.
Clarke, I.C., Manaka, M., Green, D.D., William, P., Pezzotti, G., Kim, Y.H., 2003. Current status pf Zirconia used in total hip implants. J. Bone Joint Surg. Am. 4, 73–84 2003.
Curtis, A.R., Wright, A.J., Fleming, G.J., 2006. The influence of surface modification techniques on the performance of a Y-TZP dental ceramics. J. Dent. 195–206.
Gailard, Y., Jimenez-Pique, E., Soldera, F., Mucklich, F., Anglada, M., 2008. Quantification of hydrothermal degradation in zirconia by nanoindentation. Acta Mater. 16, 4206–4216.
Guicciardi, S., Shimozone, T., Pezzotti, G., 2007. Ageing effects on the nanoindentation response of sub-micrometric 3Y-TZP ceramics. J. Mater. Sci. 42, 718–722.
Inokoshi, M., Zhang, F., De Munck, J., Minakuchi, S., Naert, I., Vleugels, J., et al., 2014. Influence of sintering conditions on low-temperature degradation of dental zirconia. Dent. Mater. 30, 669–678.
Jimenez-Pique, E., Ramos, A., Munoz-Tabares, J.A., Hatton, A., Soldera, F., Mucklich, F., et al., 2012. Focused ion beam tomography of zirconia degraded under hydrothermal conditions. J. Eur. Ceram. Soc. 32, 2129–2136.
Karakoca, S., Yilmaz, H., 2009. Influence of surface treatments on surface roughness, phase transformation, and biaxial flexural strength of Y-TZP ceramics. J. Biomed. Mater. Res. B 91, 930–937.
Keuper, M., Eder, K., Berthold, C., Nickel, K.G., 2013. Direct evidence for continuous linear kinetics in the low-temperature degradation of Y-TZP. Acta Biomater. 1, 4826–4835.
Kobayashi, K., Kuwajima, H., Masaki, T., 1981. Phase change and mechanical properties of ZrO2-Y2O3 solid electrolyte after ageing. Solid State Ion. 3, 489–493.
Kohal, R.J., Wolkewitz, M., Tsakona, A., 2011. The effects of cyclic loading and prepatation on the fracutre strength of zirconium-dioxide implants: an in vitro investigation. Oral Implant. Res. 22, 808–814.
Kohorst, P., Borchers, L., Strempel, J., Stiesch, M., Hassel, T., Bach, F.-W., Hubsch, C., 2012. Low-temperature degradation of different zirconia ceramics for dental applications. Acta Biomater. 8, 1213–1220.
Kuusisto, N., Vallittu, P.K., Lassila, L.V.J., Huumonen, S., 2015. Evaluation of intensity of artifacts in cone beam computer tomography by radiopacity of composite filling material and simulation models of implants. Dentofac. Radiol. 44.
Lawn, B., 1993. Fracture of Brittle Solids. national institute of standards and technology, *Maryland Cambridge university press*.
Lawson, S., 1995. Environmental degradation of zirconia ceramics. J. Eur. Ceram. Soc. 485–502.
Luciana, M.S., Georgios, A.K., Alex, E.P., Whasun, O.C., Dlan, M.D., 2017. Increased levels of dissolved titanium are associated with Peri-implantitis- a cross-sectional study. J. Periodontol. 5, 436–442.
Lughi, V., Sergo, V., 2010. Low temperature degradation-aging-of zirconia: a critical review of the relevant aspects in dentistry. Dent. Mater. 26, 807–820 2010.
Marro, F.G., Anglada, M., 2012. Strengthening of vickers indented 3Y-TZP by hydrothermal ageing. J. Eur. Ceram. Soc. 32, 317–324.
Monzavi, M., Noumbissi, S., Nowzari, H., 2016. The impact of in vitro accelerated aging, approximating 30 and 60 Years in vivo, on commercially available zirconia dental implants. Clin. Implant Dent. Relat. Res. 2, 245–252.
Morneburg, T.R., Pröschel, P.A., Sep-Oct 2003. In vivo forces on implants influenced by occlusal scheme and food consistency. Int. J. Prosthodont. (IJP) 16 (5), 481–486 in eng.
Osman, R., Swain, M., 2015. A critical review of dental implant materials with an emphasis on titanium versus zirconia. Materials 8 (3), 932–958.
Piconi, C., Maccauro, G., 1999. Zirconia as a ceramic biomaterial. Biomaterials 20, 1–25.
Sanon, C., Chevalier, J., Douillard, T., Kohal, R.J., Coelho, P.G., Hjerppe, J., Silva, N., 2013. Low temperature degradtion and reliability of one-piece ceramic oral implants with a porous surface. Dent. Mater. 29, 389–397.
Sanon, C., Chevalier, J., Douillard, T., Cattani-Lorente, M., Scherrer, S.S., Gremillard, L., 2015. A new testing protocol for zirconia dental implants. Dent. Mater. 31.
Spies, Benedikt Christopher, Nold, Julian, Vach, Kirstin, Kohal, Ralf-Joachim, 2016. Two-piece Zirconia oral implants withstand masticatory loads: an investigation in the artificial mouth. J. Mech. Behav. Biomed. Mater. 53, 1–10.
Tsubakino, H., Nozato, R., Hamamoto, M., 1991. Effect of alumina addition on the tetragonal to monoclinic phase transformation in zirconia-3 mol% yttria. J. Am. Ceram. 74, 440–443.
Van Velzen, F.J., Ofec, R., Schulten, E.A., Ten Bruggenkate, C.M., 2015. 10-year survival rate and the incidence of peri-implant disease of 374 titanium dental implants with a SLA surface: a prospective cohort study in 177 fully and partially edentulous patients. Clin. Oral Implant. Res. 26 (10), 1121–1128.
Yoshimura, M., Noma, T., Kawabata, K., SOmiva, S., 1987. Role of H_2O on degradation process of Y-TZP. J. Mater. Sci. Lett. 6, 465–467.